Radiocarbon (2026), **68**, pp. 264–280
doi:10.1017/RDC.2025.10186

CAMBRIDGE UNIVERSITY PRESS

RESEARCH ARTICLE

Investigating potential radiocarbon anomalies around the time of the Minoan eruption of Thera: A new high-resolution dataset from Groningen

Pınar Erdil[1,2], Margot Kuitems[1], Andrea Scifo[1], David Brown[3] and Michael W. Dee[1]

[1]Centre for Isotope Research, ESRIG, University of Groningen, Nijenborgh 6, 9747 AG Groningen, The Netherlands, [2]Groningen Institute of Archaeology, University of Groningen, Poststraat 6, 9712 ER Groningen, the Netherlands and [3]School of Natural and Built Environment, Queens University Belfast, Belfast, BT7 1NN, Northern Ireland, UK
Corresponding author: Pınar Erdil; Email: p.erdil@rug.nl

Received: 22 April 2025; **Revised:** 07 November 2025; **Accepted:** 20 November 2025; **First published online:** 12 February 2026

Keywords: calibration curve; radiocarbon dating; Thera eruption; tree rings

Abstract
The date of the Thera eruption has been a subject of intense debate since the mid-20th century. In recent years, the disagreements have escalated with the introduction of IntCal20. The increased number of annual measurements around the time period of the eruption has highlighted potential fluctuations in the atmospheric radiocarbon record, shedding new light on the date of the disastrous event. The Centre for Isotope Research in Groningen has already contributed data from this time period to IntCal20, and here, we report a new set of annual data of approximately 90 radiocarbon measurements between 1660 and 1507 BCE. We investigate the potential anomalies in the calibration curve and compare our dataset with those from other leading laboratories. Although we do not find compelling evidence of any rapid increases in radiocarbon production during this period, the results do point to the presence of minor differences between datasets which could be species, region or laboratory pretreatment related. By quantifying such offsets, we assess their impact on chronological models related to the eruption of Thera.

Introduction

The 2020 update to the international radiocarbon (^{14}C) calibration curve (IntCal20) introduced far greater detail to the record through a substantial increase in measurements on individual tree rings. Since then, annual resolution measurements have revealed new insights, such as detailed information on past ^{14}C concentrations in the atmosphere which was previously obscured by coarser measurements on multi-ring blocks of 5, 10, or 20 years.

Such investigations have been particularly crucial for studies on the 2nd millennium BCE, a period that had already received considerable attention due to the controversial dating of the Minoan eruption of Thera (modern-day Santorini). In fact, the mid-2nd millennium BCE has now become one of the most extensively studied and best ^{14}C-dated periods in history (Manning 2022, 2024a, 2024b; Pearson et al. 2018, 2023).

The Minoan eruption was one of the largest volcanic events of the Holocene (Johnston et al. 2014; Sigurdsson et al. 2006). It potentially had environmental, cultural, political and economic consequences for the contemporary cultures in the region, and putatively triggered earthquakes and tsunamis that reached as far as Crete and the shores of Anatolia (Aydar et al. 2021; Bruins et al. 2008; Lespez et al. 2021; McCoy and Heiken 2000; Şahoğlu et al. 2022). Some argue the eruption even instigated a climatic downturn, leading to widespread crop failures, famine, migration, and disruption of local economies and trade networks (Driessen and Macdonald 2000; Foster and Ritner 1996; Friedrich and

Sigalas 2009; LaMoreaux 1995; Soles 2007; White & Humphreys 1994). Indeed, the aftermath of the eruption, especially for the island of Crete, either in terms of direct destruction (Luce and Bolton 1976; Marinatos 1939) or more nuanced arguments around long-term socio-economic disruption (Driessen 2019; Druitt et al. 2019; Manning and Sewell 2002; Pyle 1997), has now been a topic of debate for more than a century.

The core of the debate lies in determining the exact eruption date. Archaeological synchronisms between Egypt, Greece and the Levant place the eruption around 1500 BCE (Bietak 2013; Höflmayer 2012; Warren 2009, 2010; Warren and Hankey 1989), whereas most of the ^{14}C evidence suggests a date closer to 1600 BCE (Bruins and van der Plicht 2014; Friedrich et al. 2006; Höflmayer 2012; Manning 2022; Manning et al. 2006, 2014). The 100-year discrepancy between the two scenarios may seem trivial in some contexts but, in this case, it is pivotal to unravelling the long-term impact of this event. Recently, the new high-resolution data on tree rings have reignited the debate on the ^{14}C date of the eruption. It has been revealed that the international calibration curve has suffered from offsets, either localized (Dee et al. 2010; Manning et al. 2018, 2020a, 2020b) or global (Pearson et al. 2018; Regev et al. 2024). In particular, a clear disparity was found between IntCal13 and IntCal20 over the course of more than 100 years (ca. 1660 to ca. 1540 BCE) (Pearson et al. 2018). Such discrepancies can result from a variety of causes. Laboratory factors, data artefacts, or differences in latitude or growing season among the various tree species are all possible sources, and all could cause the ^{14}C dates from the eruption to be incorrect.

A couple of specific anomalies in ^{14}C concentration have been suggested for the years 1557 and 1528 BCE, based on data from bristlecone pine (*Pinus longaeva*) in California (Pearson et al. 2018, 2020b). In the same publication, the feature in 1557 BCE is not observed in oak (*Quercus sp.*) measurements from Ireland; however, the datasets from both species show a significant increase in Δ^{14}C (‰) values around 1528 BCE. These are potential Miyake Events, which are sudden spikes in ^{14}C production associated with intense solar activity (Bard et al. 2023; Brehm et al. 2022; Büntgen et al. 2018; Miyake et al. 2012, 2013). Miyake Events can serve as time-markers in assigning historical events to a single year (Kuitems et al. 2020a, 2022; Maczkowski et al. 2024). So far, five events have been confirmed, although the precise criteria for confirmation have not yet been universally agreed. What is common to these five cases is that they have been found in independent dendrochronological archives, from different parts of the world, by multiple laboratories. Equivalent anomalies have also all been found in the same years in ice core records. These five cases correspond to: 774 CE (Miyake et al. 2012), 993 CE (Miyake et al. 2013), ~664 BCE (O'Hare et al. 2019; Panyushkina et al. 2024; Park et al. 2017), 5259 BCE and 7176 BCE (Brehm et al. 2022). Additional spikes have also been proposed but not yet confirmed, including in 5410 BCE (Miyake et al. 2021), 1052 CE and 1279 CE (Brehm et al. 2021). The presence of a spike in 1557 or 1528 BCE could facilitate a precise date for the eruption, which would thus clarify the consequences of the eruption, help secure the chronology of the Eastern Mediterranean region, and allow us to understand the political and cultural shifts that developed after this massive event (Kutschera 2020; McCoy 2009).

Many laboratories around the world have contributed ^{14}C dates to IntCal20 for this time period. Currently, the calibration data comes from measurements from Germany, the Netherlands, Ireland, and California. New annual measurements for IntCal20 were provided by the University of Arizona; the Swiss Federal Institute of Technology, Zurich; the Curt-Engelhorn-Centre for Archaeometry, Mannheim; and Aarhus AMS Centre, University of Aarhus. These augmented the extant multi-ring measurements from Heidelberg University Radiocarbon Laboratory (now Central Radiocarbon Laboratory of Heidelberg University); the Quaternary Isotope Lab, University of Washington; and the 14CHRONO Centre, Queens University Belfast. In comparison, University of Groningen (laboratory code: GrM) has contributed 18 ^{14}C dates to the calibration record over this period (Kuitems et al. 2020b), which were both in annual and multi-year resolution.

In this paper, our aim is to provide considerably more annual data over this controversial period measured by the Centre for Isotope Research (CIO), Groningen. Building upon Kuitems et al. (2020b), we present new ^{14}C measurements on dendrochronologically dated wood from the Netherlands and

https://doi.org/10.1017/RDC.2025.10186 Published online by Cambridge University Press

Table 1. *List of dendrochronological samples selected and measured for ^{14}C content in this paper*

Sample			Date range	Number of ^{14}C
ID	Location	Species	(BCE)	results*
Q8046	Garry Bog, Northern Ireland, UK	Oak	1600–1580	29
Q5392	Sentry Hill, Northern Ireland, UK	Oak	1610–1595	16
Q1933	Garry Bog, Northern Ireland, UK	Oak	1560–1507	43
BOF00041**	Bodegraven, The Netherlands	Oak	1596–1588	4
			1592–1591	1 (2-year block)
			1660–1612	9**
			1645–1565	9 (10-year blocks)**
Total			1660–1507	111

*Annual samples unless otherwise stated.
**See Kuitems et al. (2020b) for more detail.

Northern Ireland, UK. Our analysis focuses on investigating any proposed offsets in ^{14}C concentration and exploring the likelihood of a Miyake Event that could serve as an exact time marker for this period. Specifically, we compare our dataset with respect to IntCal20, other laboratories, tree species, and the latitude of the sample origin.

Materials and methods

Sample material

All of the tree-ring samples used in this study are listed in Table 1. Eighteen ^{14}C measurements on sample (BOF00041) from Bodegraven, the Netherlands, were published by Kuitems et al. (2020b), alongside detailed dendrochronological information on the sample. These data are already included in the IntCal20 database. Here, we have extended this dataset by five measurements. The rest of our new measurements were obtained on dendrochronologically dated wood from Garry Bog (55°06'N, 6°31'W) and Sentry Hill (54°33'N, 6°11'W), Northern Ireland, UK. In this case, *Quercus sp.* tree rings were dissected from three different samples from these sites (Q8046, Q5392 and Q1933). Their early and late wood fractions were not separated because the ring widths were too narrow. A total of 93 new tree rings were pretreated and analysed for their ^{14}C content.

Pretreatment

All the samples were subjected to Groningen's α-cellulose extraction protocol, details of which can be found in Dee et al. (2020). Put simply, the procedure involves a strong acid-base-acid (ABA) sequence (1.5 M HCl, 80 °C, 20 min; 17.5 w/vol, NaOH, RT, 60 min ultrasonicated under N_2 atmosphere; 1.5 M HCl, 80 °C, 20 min) with an additional bleach step (1.5% w/vol $NaClO_2/H^+$, pH=3, 80 °C, 16 hr). The resulting product is freeze-dried, weighted into tin capsules, combusted and graphitized (Dee et al. 2020). The ^{14}C measurements are then obtained using a MICADAS AMS (Synal et al. 2007).

Results and discussion

Experimental results

Here, we present 93 new high-precision ^{14}C measurements at annual-resolution covering a total span of 153 calendar years. Due to practical constraints, such as very narrow tree rings, it was not possible to obtain a result for every single year. The list of the ^{14}C measurements from all tree samples is given in

https://doi.org/10.1017/RDC.2025.10186 Published online by Cambridge University Press

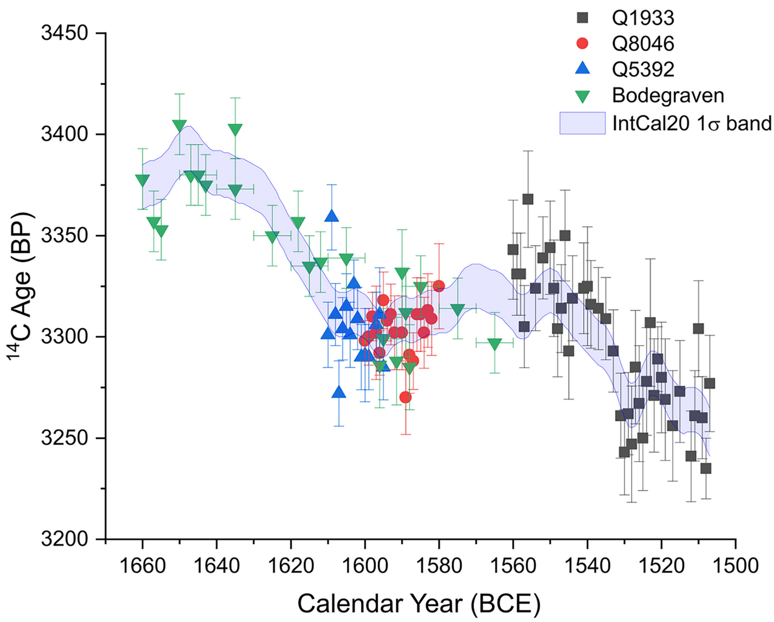

Figure 1. *All Groningen (GrM) measurements on tree rings from Bodegraven, the Netherlands and Garry Bog and Sentry Hill, Northern Ireland, UK (Q1933, Q8046, Q5392). Different colors represent different samples and tree-ring chronologies.*

the Supplementary Material Tables S1–S4. All of these data are plotted in Figure 1 in comparison with IntCal20 (Reimer et al. 2020).

Comparisons with IntCal and other laboratories

To analyse our dataset for any potential systematic offsets, we compared it across laboratories, tree species, and based on the latitude of the sample origin. To maintain a controlled approach, only measurements from Northern Ireland were used (the data from the Netherlands were excluded), ensuring that all comparisons were conducted using the similar latitude (55°–54°N) and species (*Quercus sp*). In order to create one continuous dataset, we calculated the weighted mean of multiple measurements from the same calendar year for all the wood samples (i.e. the weighted mean of measurements on samples Q8046 and Q5392). There were 12 such averaged results and each passed the χ^2 test (see Supplementary Material Table S5) (Ward and Wilson 1978). After applying the weighted mean, a total of 70 single-year measurements were used in the offset comparisons.

Initially, we compared our dataset directly to IntCal20. As seen in Figure 1, our data closely agrees with the 1σ band of this reference dataset. The GrM data does not show any statistically significant offset (0 ± 3 ^{14}C years). However, the calibration curve is a statistically smoothed dataset that averages out fluctuations in ^{14}C concentration; certain details may be obscured in the process. We therefore shifted our focus to the composite datasets for a more comprehensive analysis. We tested for differences between GrM and the single-year measurements from the Curt-Engelhorn-Centre for Archaeometry, Mannheim (MAMS; oak from Knetzgau, Germany), the Swiss Federal Institute of Technology (ETH; oak from Timahoe West, Ireland), and the University of Arizona (AA; bristlecone pine from Sheep Mountain, California, USA, and oak from Timahoe West, Ireland). Additionally, we tested other relevant datasets from the same time period that are not incorporated into IntCal20. These provide alternative parameters for comparison, such as different latitude and species (AA; juniper from Gordion,

https://doi.org/10.1017/RDC.2025.10186 Published online by Cambridge University Press

Table 2. *Comparisons between the GrM annual dataset on oak from Northern Ireland, UK (55°–54°N) corresponding to IntCal20, ETH, MAMS, and AA measurements. Juniper data from Turkey (Pearson et al. 2020a) and kauri data from New Zealand (Pearson et al. 2020b) are not incorporated in the IntCal20 dataset. All the datasets listed below were prepared using holocellulose extraction, except for GrM, where α-cellulose was the preferred extract.*

	Sample				Weighted mean offset	
GrM vs.	location	Species	Approximate latitude	# of ^{14}C dates compared	^{14}C yr	±
IntCal20	Northern Hemisphere	Various	—	70	0	3
ETH	Timahoe West, Ireland	Oak	53°N	70	5	3
MAMS	Knetzgau, Germany	Oak	49°N	66	–4	3
AA	Sheep Mountain, California, USA	Bristlecone pine	37°N	69	–10	3
AA	Timahoe West, Ireland	Oak	53°N	48	1	5
AA	Gordion, Turkey	Juniper	39°N	70	–17	4
AA	Gibson's Farm, Dargaville, New Zealand	Kauri	35°S	40	–35	5

Turkey, and kauri from Gibson's Farm, Dargaville, New Zealand) (Pearson et al. 2020a, 2020b). The weighted mean offsets between the various datasets are presented in Table 2.

The offset of –35 ± 5 ^{14}C years with the kauri data confirms the difference in the ^{14}C concentration in the atmosphere between the Northern and Southern Hemispheres (NH, SH) (Hogg et al. 2020; –36 ± 27 ^{14}C years). Otherwise, GrM data shows statistically significant offsets relative to the AA measurements on bristlecone pine from Sheep Mountain (–10 ± 3 ^{14}C years) and juniper from Gordion (–17 ± 4 ^{14}C years), as the 2σ ranges for these offsets do not overlap zero. In contrast, the GrM offsets relative to ETH oak (5 ± 3 ^{14}C years) and MAMS (–4 ± 3 ^{14}C years) datasets are not statistically significant.

The variances obtained are unlikely to result from inter-laboratory offsets, as GrM does not show a significant difference with AA measurements on oak (1 ± 5 ^{14}C years). However, it should be noted that the absolute age of the juniper sample is based on a wiggle-matched sequence, even though the calendar year match is quite precise (± 4 years for the sequence's final ring). Thus, our offset calculations might not reflect a direct year-to-year comparison.

The offset in ^{14}C years observed between GrM and AA datasets from Gordion and Sheep Mountain (approximately 15°–16° and 17°–18° difference with Northern Ireland datasets respectively) accord with the latitudinal gradient proposed by Büntgen et al. (2018). Their research has highlighted that the ^{14}C concentrations are higher at latitudes above 60°, identifying a "meridional north–south gradient of declining average ^{14}C values" (Büntgen et al. 2018). The atmospheric ^{14}C levels can vary across different atmospheric circulation zones, which are defined through carbon cycle modeling and ^{14}C dating over the Bomb Period (Hua et al. 2013, 2022). Such factors are particularly relevant to dating of the Thera eruption, as the island is located in NH Bomb Zone 2, much farther south than the trees that make up the calibration curve, which predominantly grew in NH Bomb Zone 1. Any latitude variation in ^{14}C levels on the calibration curve could therefore influence the results.

To assess this effect, we plotted the mean $\Delta^{14}C$ (‰) values in relation to latitude, following a similar approach to Büntgen et al. (2018, p.4), as shown in Figure 2. We used 66 ^{14}C measurements from 1610 to 1510 BCE across the five NH latitudes listed in Table 2. This subset was selected as it represents the common calendar years present across all datasets. Our results reveal a similar pattern to their analysis

https://doi.org/10.1017/RDC.2025.10186 Published online by Cambridge University Press

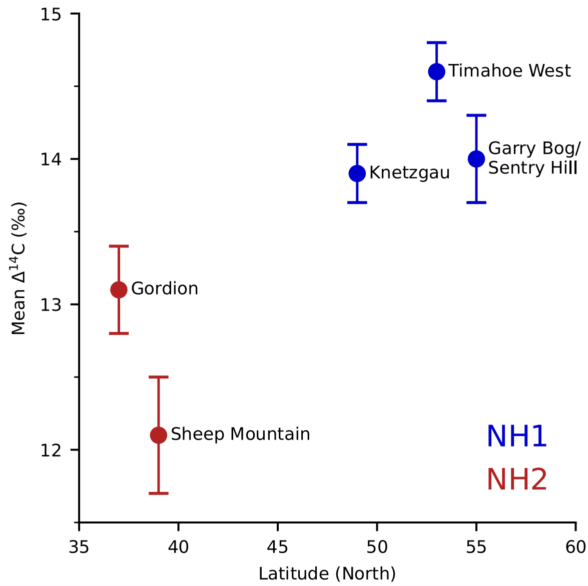

Figure 2. *Scatter plot of the mean* ^{14}*C values by latitude. The mean value of 66* ^{14}*C measurements on tree rings between 1510–1610 BCE. Datasets are from Knetzgau, Timahoe West and Garry Bog/Sentry Hill (NH1); Sheep Mountain and Gordion (NH2).*

with a strong positive correlation between latitude and the mean $\Delta^{14}C$ values, higher latitudes exhibiting higher ^{14}C concentrations. It should be acknowledged that our dataset is limited to only five groups.

However, when comparing samples from different latitudes, several lurking variables could not be controlled for. These include variations in local growing season, tree physiology and even differences in laboratory pretreatment. At higher latitudes, trees tend to grow primarily in mid-to-late summer, whereas at lower latitudes, growth occurs earlier, between spring and early summer (Kromer et al. 2001; Manning 2024a). This coincides with the seasonal fluctuations of atmospheric ^{14}C levels, reaching a minimum in late winter and a maximum in late summer for NH (Kitagawa et al. 2004 ; Levin and Kromer 2004; Manning et al. 2018, 2020b). As a result, trees from higher latitudes, such as Irish and German oaks, take in carbon during this maximum, potentially making their ^{14}C ages slightly younger. In contrast, trees from lower latitudes, such as Turkish juniper, tend to absorb carbon earlier in the year, leading to slightly older ages (Dee et al. 2010; Kromer et al. 2001). This is consistent with what we present in Table 2 and Figure 2, with measurements on higher latitude trees exhibiting younger ages. Bristlecone pine from California, however, has a particularly short and distinct growing period in summer because of the high altitudes at which it grows (Beasley and Klemmedson 1980; Pearson et al. 2020b). It should thus primarily record the summer maximum in ^{14}C values and should align more closely with boreal wood rather than with trees from similar latitudes, such as Turkish juniper. Yet, the ^{14}C levels in bristlecone pine appear more comparable to Turkish juniper, indicating that additional factors may be driving the observed offsets.

Another such parameter is differences in laboratory approaches and pretreatment protocols. For example, the observed offsets could relate to differences between the earlywood and latewood fractions of trees. Due to seasonal atmospheric fluctuations and carbon storage dynamics, it has been suggested that NH latewood tends to contain more ^{14}C, and hence appears younger, than earlywood (McDonald et al. 2019). While this difference was not statistically significant within 2σ, McDonald et al. (2019) report a 96% probability that latewood is more enriched. This observation is qualitatively consistent

https://doi.org/10.1017/RDC.2025.10186 Published online by Cambridge University Press

with a recent study on tree physiology using samples from the post-bomb era by Kromer et al. (2024). They claim that earlywood in most species is formed from stored older carbon, whereas latewood is primarily derived from products of more recent photosynthesis. Among the datasets listed in Table 2, only the Timahoe West samples are separated by wood fraction, with only latewood used, while the rest are measurements on full tree rings. Consistent with the aforementioned research on ring fractions, as shown in Figure 2, this dataset exhibits the highest mean $\Delta^{14}C$ (‰) values, appearing younger than the rest. Such differences could contribute to small but consistent offsets, and further controlled studies are needed.

Finally, variations in the different pretreatment methods should also be taken into account. For example, the protocols used by Friedrich et al. (2020) and Pearson et al. (2020b) involve holocellulose, while our GrM dataset is the only one analysed using α-cellulose. Even though it requires a longer and harsher procedure than simple holocellulose extraction (Khumalo et al. 2024) and therefore may be problematic for poorly preserved samples (Capano et al. 2018; Jędrzejowski et al. 2024), α-cellulose is a more discerning protocol, and results in higher removal of lignin and other potential contaminants (Hoper et al. 1997; Rinne et al. 2005). One previous research found no statistically significant difference between these two pretreated fractions, although the ^{14}C measurements on α-cellulose from the same tree rings were consistently older than those on holocellulose in their dataset (Lange et al. 2019). It therefore remains unclear which fraction yields the most representative age.

In Table 2, there is no significant inter-laboratory offset between our data and MAMS, ETH or AA measurements on the same wood species (oak) from northern Europe (Knetzgau, Timahoe West). This was expected due to the minimal differences in latitude between the sampling locations and the use of the same species. However, for the remaining comparisons, multiple variables, such as species and latitude differences, growing seasons, atmospheric ^{14}C fluctuations, and pretreatment techniques, make it challenging to isolate the exact cause of the observed offsets. Nevertheless, the offsets between these different datasets exert only a limited influence on calibrations using IntCal, since the curve is constructed as a statistically smoothed average of all these records.

Short-term features in mid-16th century BCE

To investigate the veracity of the possible Miyake Events in 1557 and 1528 BCE, we first zoom in to our dataset and extract 50 years of measurements over the period 1560–1510 BCE. Once again, we compare the data obtained by our laboratory with some of the IntCal20 composite datasets over this window (see Figure 3). Our GrM measurements align more closely with those of ETH than AA or MAMS. We do not observe the specific anomaly reported by Pearson et al. (2020b) around 1558-1557 BCE, similar to the ETH, AA oak and MAMS datasets. However, the GrM, ETH and AA bristlecone pine data all show a short-lived but comparatively sharp decrease between 1557-1556 BCE (GrM 8‰; ETH 6‰; AA bristlecone pine 9‰).

Turning to the proposed anomaly around 1528 BCE, there is a very similar pattern between all laboratories around 1534–1515 BCE, where a steep rise in ^{14}C levels is indeed observed. This increase begins in 1533 and peaks between 1530 and 1528 BCE and subsequently declines in all the datasets. The peak rise amounts to approximately 5–6‰ for GrM; 7‰ for ETH; 8‰ for AA bristlecone pine; 6–7‰ for MAMS; and 8‰ for AA oak in Figure 3b. While the value is lower than the confirmed Miyake Events listed in the Introduction; it is comparable to the proposed events of 1052–1053 CE (5.9‰) and 1279–1280 CE (6.5‰) (Brehm et al. 2022), the existence of which has latterly been disputed by Scifo et al. (2024). Further, the values show an exponential increase over 4–5 years rather than an abrupt rise or a spike like a Miyake Event, similar to the rise between 541–546 CE (6‰) reported by Scifo et al. (2024).

While the gradual rise in ^{14}C levels ca. 1530 BCE lacks the characteristics of a Miyake Event, there seems to be a particular pattern evident in all the datasets. The shape of the data between 1534 and 1515 BCE becomes visually apparent after applying data smoothing, as shown in Figure 4. We used the Loess

https://doi.org/10.1017/RDC.2025.10186 Published online by Cambridge University Press

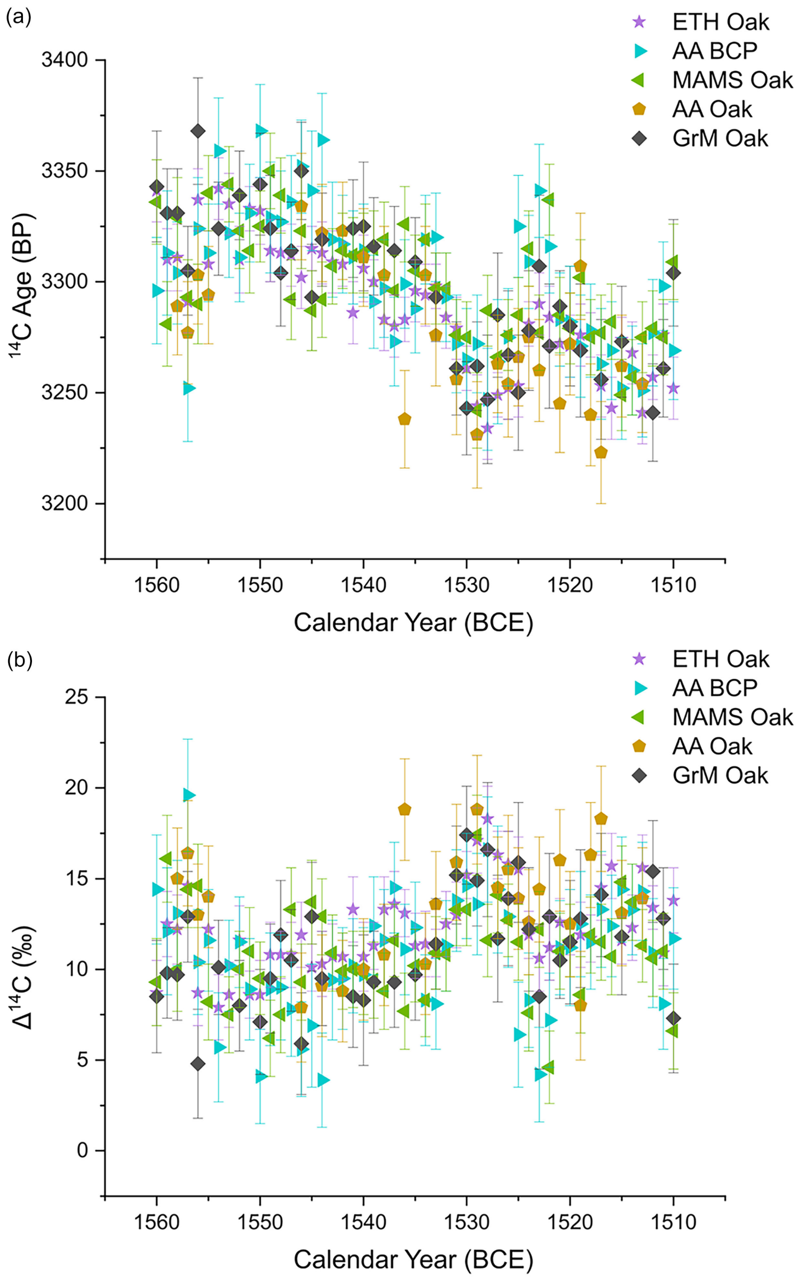

Figure 3. *Single year measurements between 1560–1510 BCE from GrM (this study), along with ETH, AA (Pearson et al. 2018, 2020b), and MAMS (Friedrich et al. 2020) showing (a) ^{14}C data (b) corresponding Δ^{14}C values.*

nonparametric method of data smoothing since the GrM, MAMS and AA oak datasets do not have evenly spaced x-axis values, as some calendar years were skipped. Although the intensity of the ^{14}C concentration varies over this period, for instance AA bristlecone pine and MAMS show elevated levels between 1525–1520 BCE, the overall wiggle pattern is consistent across all labs (GrM, AA, ETH, and MAMS) and latitudes (Ireland, Germany, California). This pattern may still offer a time marker of similar value, provided the sample in question has the right characteristics (i.e. a series of single-year

https://doi.org/10.1017/RDC.2025.10186 Published online by Cambridge University Press

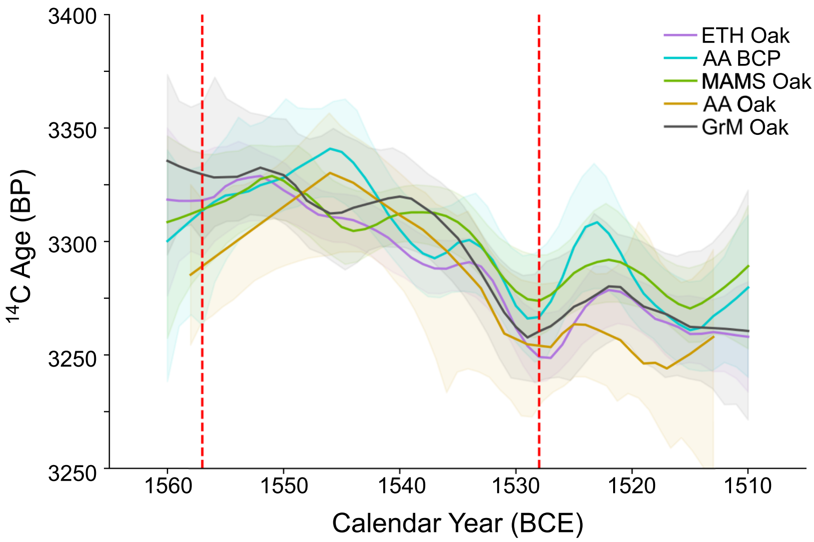

Figure 4. *The ^{14}C data shown in Figure 3 smoothed using the Loess nonparametric method. The red lines mark the previously reported anomalies on 1557 and 1528 BCE. A similar wiggle fluctuation pattern is visible across all datasets between 1534 and 1515 BCE.*

samples) for its identification. For instance, if the eruption had occurred after 1530 BCE, this undulation would almost certainly be evident in the data.

Potential candidates for Miyake Events can also be examined using carbon box models (see Scifo et al. 2024; Brehm et al. 2025). We investigated the proposed anomaly in 1528 BCE using the open-source Python package `ticktack` on the extracted data over the period 1560–1510 BCE on Garry Bog only (Zhang et al. 2022; Sharma et al. 2023). This modeling library is designed to analyse Δ^{14}C (‰) values, detect potential anomalies and summarize ^{14}C production data. Detailed explanations of this package and its application to different datasets are provided in Zhang et al. (2022). We used the 22-box model of Brehm et al. (2021), already implemented within `ticktack`, and applied `spike only` command to test whether there is a sudden rise on ^{14}C production on 1528 BCE (see Supplementary Material Table S6 for model specifications). This method is specifically designed to identify potential events within the input dataset.

The results of the modeling are presented in Figure 5. First, we display the model estimates in terms of Δ^{14}C (‰) in Figure 5a. The key posterior parameters from this analysis, the Start Date, Duration, and Q, with the latter representing integrated ^{14}C yields over the observed rise, are shown in Figure 5b. A small potential increase in ^{14}C production of approximately 1.6 ^{14}C atoms/cm^2/s per year is estimated to occur around 1532.7 ($^{+1.6}_{-1.1}$ years) BCE. In comparison, the 775 event produced 6.4 ^{14}C atoms/cm^2/s per year (Scifo et al. 2024), so our data shows an increase in production rate that is roughly four times lower. Our result is comparable with the 1052 CE (1.4 atoms/cm^2/s), 1279 CE (1.1 atoms/cm^2/s), and 540s CE (1.7 atoms/cm^2/s) event candidates. All these latter features are ambiguous and characterized by low production rates and unresolved start dates. Indeed, they may simply represent normal variations in solar modulation, as reported by Scifo et al. (2024). Furthermore, we do not have a ^{14}C measurement for the year 1532 BCE, as our data skips from 1533 to 1531 BCE, which may have influenced the model's interpretation of a possible rise in ^{14}C production. Nevertheless, the models exclude 1528 BCE as a starting date for a Miyake Event at 95.4% probability (Figure 5b).

In summary, there is only weak evidence to suggest a significant and sudden ^{14}C production event comparable with the previously confirmed, globally replicated Miyake Events. Hence, there is no specific tie point here for chronology, particularly for the Thera eruption.

https://doi.org/10.1017/RDC.2025.10186 Published online by Cambridge University Press

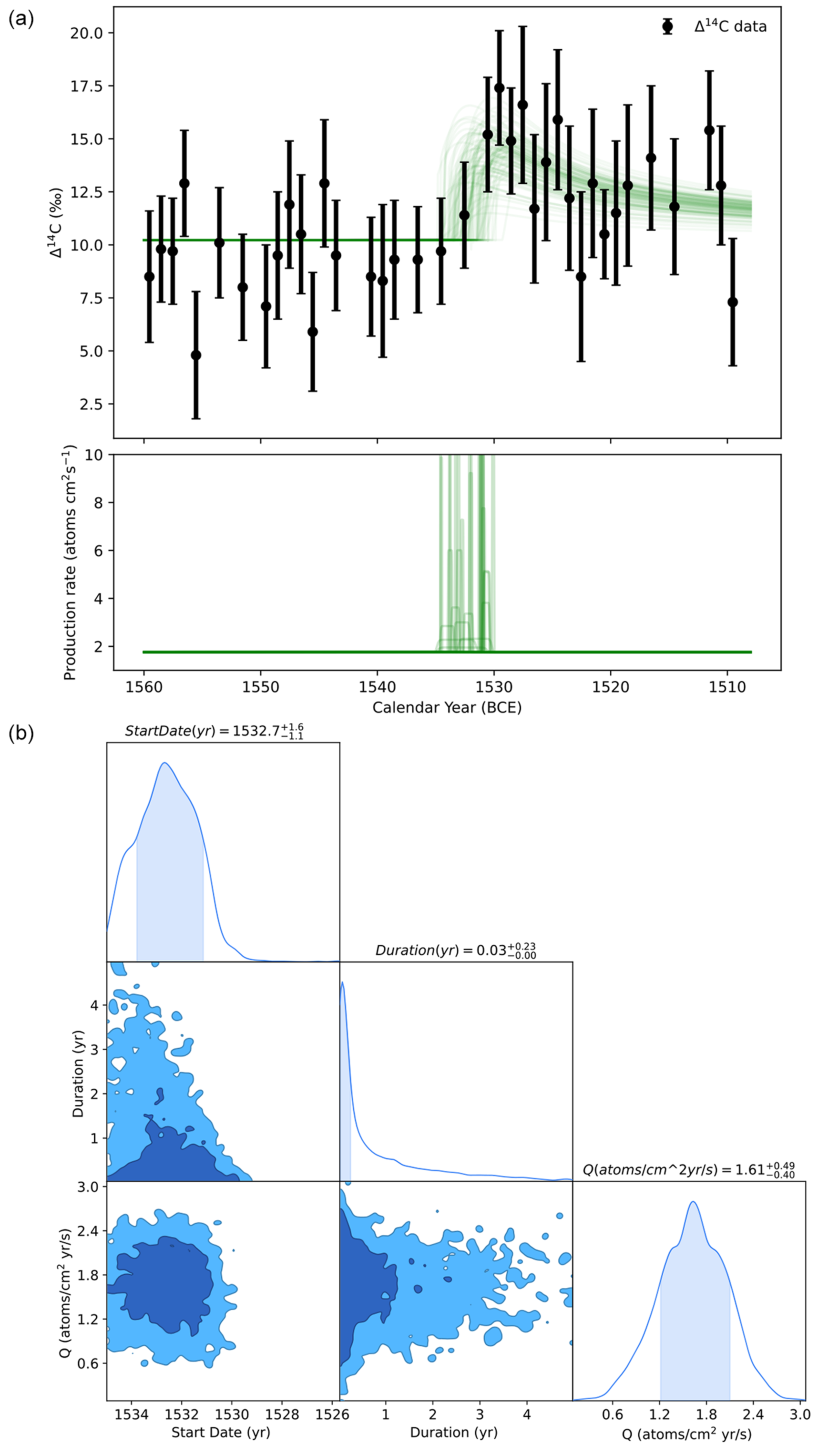

Figure 5. *Focus on 1560–1510 on new GrM ^{14}C data, all dates are in BCE. (a) The possible Δ^{14}C (‰) estimates of the event from spike only model results shown in green lines (b) Corner plot of the posterior parameters from the* `ticktack` *model showing 68.2% (dark blue) and 95.4% (light blue) probability ranges.*

https://doi.org/10.1017/RDC.2025.10186 Published online by Cambridge University Press

Modeling of the archaeological datasets related to the eruption of Thera

The smoothed curves on Figure 4 reveal elevated ^{14}C levels in the AA bristlecone pine and MAMS datasets after 1530 BCE, with measurements reaching as much as 3300 BP. In contrast, the other datasets do not show such high ^{14}C ages post-1530 BCE. Such features could also influence the ^{14}C calibrations for the Thera eruption. To test this, we prepared two new calibration curves: one that incorporated single-year IntCal20 data with the new GrM data (GrM inc.), and another based solely on AA bristlecone pine and MAMS data (AA BCP & MAMS-only). These two test curves are simply the weighted average of the measurements for each calendar year from the single-year datasets.

Using IntCal20 and these two test curves, we employed OxCal software (Bronk Ramsey 2009a, version 4.4) to rerun the `R_Combine` analysis of 24 ^{14}C dates on short-lived plant samples from the Akrotiri volcanic destruction level (VDL) at Thera, excluding four problematic measurements with uncertain contexts, as discussed by Manning (2024a). The resulting calibrations using each curve are not significantly different from each other (Figure 6). The highest region of probability still falls between 1650–1600 BCE. The only difference is the GrM data introduces a slight probability for the eruption date to be earlier than the 1700s, which is not archaeologically feasible.

Apart from using `R_Combine` with the VDL dataset, we also tried modeling them simply by placing the 24 measurements under a `Phase` within two uniform `Boundary` functions. The resulting probability for the end `Boundary` for this model is given on Figure 7a. Since this model is very simple, with no specific constraints, the resulting probabilities are wider. The highest region of probability still falls in the 17th century BCE.

Additionally, we tested the applicability of the `Delta_R` adjustment to account for a potential offset for the Thera dataset in comparison to the calibration curve, in light of the results of our analysis in the previous section of this paper. As discussed earlier, the precise cause of these observed offsets could be a combination of factors, including differences in growing season, tree physiology, laboratory pretreatment, and potentially latitude. The latitudinal gradient proposed by Büntgen et al. (2018) also correlates with differences in growing season and offers a practical proxy for modeling purposes. We explore this by applying a `Delta_R` correction of 10 ± 3 which is the offset between the GrM oak vs. AA bristlecone pine measurement. This offset approximately reflects the difference between the trees that predominantly contribute to the calibration curve between 1700–1500 BCE (Irish and German oak) and the latitude of Thera. We recognise that this might be an oversimplification of multiple overlapping effects; however, latitude is the only variable we can control using the available data. With this compensation included the probability for a 16th century date for the eruption increases (Figure 7a). However, there are 882 ^{14}C measurements in total between 1700 and 1500 BCE in IntCal20 and 198 measurements come from AA bristlecone pine, representing 22% of these data. Thus, just under a quarter of the IntCal20 data used to calibrate ^{14}C dates from the Theran eruption come from the same latitude as the volcano, compared to 33% from German oak and 42% from Irish oak. So, while it seems highly likely that an offset exists, it would be significantly less than 10 ± 3 in the case where all the IntCal20 data are included. Applying this offset is less justified when using the AA BCP & MAMS-only curve, where 50% of the data in this period comes from the same latitude and would not be affected by a latitude-related offset, and we have therefore not included this version in the figures.

Since the ^{14}C calibration curve over this period is affected by a plateau (Manning 2024a), it is customary to make use of Bayesian modeling to incorporate constraints. To address this issue, we reran the most extensive model proposed by Manning (2024a) which integrates the Therasia olive shrub sequences (Pearson et al. 2023), Thera olive sequence (Friedrich et al. 2006) as well as the VDL dataset (Manning 2014; Manning et al. 2006) (see Manning 2024a for the OxCal code and the underlying rationale). However, we have adapted the code with a uniform `Boundary` instead of `Tau Boundary`

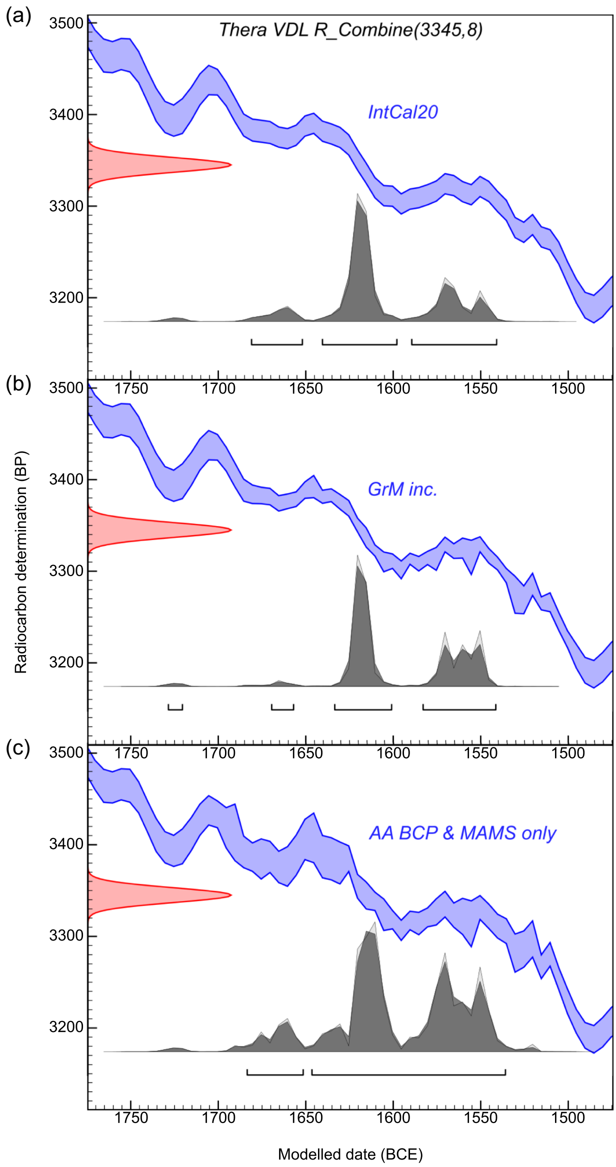

Figure 6. *Calibration of Thera Akrotiri VDL seeds dataset using* `R_Combine` *using (a) IntCal20 (b) single-year IntCal20 data incorporating the new GrM measurements (c) AA bristlecone pine and MAMS-only data.*

and also included a `General Outlier model` (Bronk Ramsey 2009b). These models were run both with and without the aforementioned `Delta_R` adjustment. While this approach introduces more constraints to the model, it allows us to overcome the impact of the plateau. The `Boundary` labelled as Eruption is plotted on Figure 7b. The 95.4% probability ranges are narrower than those of the VDL model as a result of the additional constraints. There is less probability allocated to 16th century BCE, with the highest probability again clustering around 1600 BCE. Yet, despite the elevated ^{14}C levels of AA bristlecone pine and MAMS datasets, the modeled results still do not support a timeline for the eruption as late as 1500 BCE.

https://doi.org/10.1017/RDC.2025.10186 Published online by Cambridge University Press

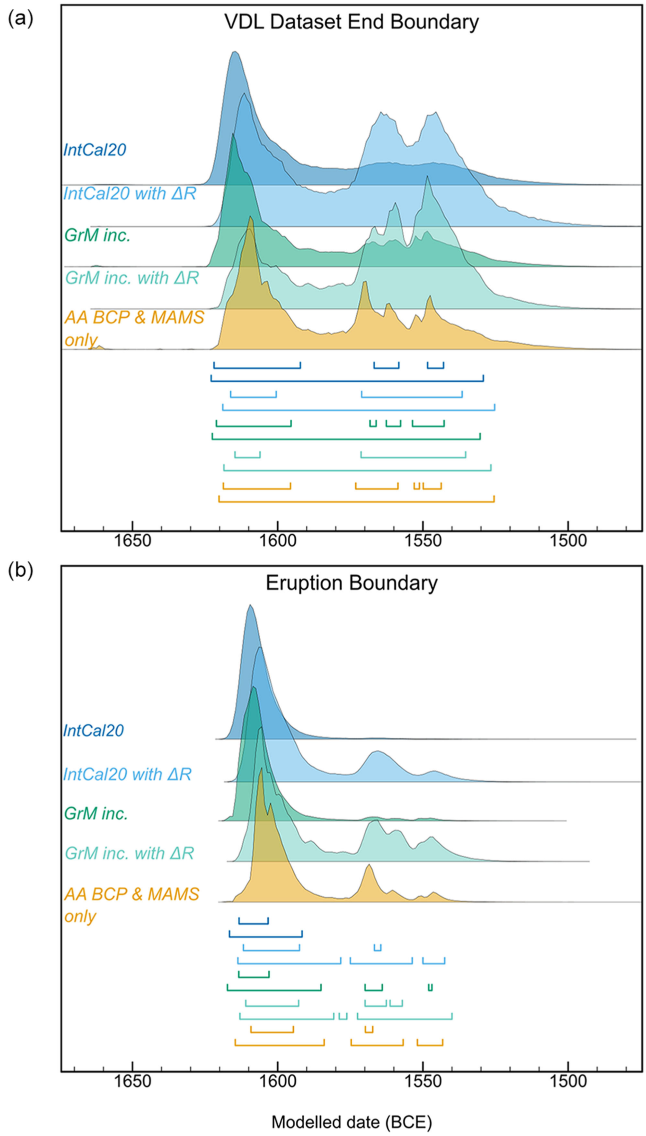

Figure 7. *Modeled results for (a) the end Boundary of Akrotiri VDL seeds, (b) the Eruption Boundary of the model by Manning (2024a) incorporating Thera olive sequence, Therasia shrub sequences and the VDL dataset, using different calibration curves and Delta_R adjustment. The models are run with three different curves: IntCal20 (blue), single-year IntCal20 data incorporating the new GrM measurements (green), and a curve using AA bristlecone pine and MAMS-only data (orange). The 68.3% and 95.4% probability ranges are shown below the graphs, following the respective color coding.*

Conclusions

The IntCal20 calibration curve is the product of extensive collaboration across multiple disciplines. This international effort is essential for achieving accuracy and precision in ^{14}C dating. Inclusion of datasets from different laboratories, as well as samples from diverse latitudes and tree species, enhances the reliability of the calibration curve and therefore the calibration process. In this context, we present new annual-resolution ^{14}C data over 1660–1507 BCE, of direct relevance to the ongoing discussion of the date of the Thera eruption.

We have compared our measurements with datasets from other leading laboratories contributing to IntCal20. While our results overlap with IntCal20, the offset analysis reveals the possibility of a seasonal, latitudinal, species or pretreatment related effect as previously discussed in literature. We do not observe any distinct features around 1557 or 1528 BCE that could serve as a definitive chronological marker for the Thera eruption. However, there is a distinctive pattern evident in ^{14}C levels between 1530–1520 BCE in all datasets, which warrants further investigation. Potentially, this pattern could be used as a fingerprint in obtaining an exact date of the eruption.

Furthermore, we reran models related to the Thera eruption from existing literature using several test calibration curves. However, even when the models are ran using a curve with elevated ^{14}C levels, the resulting probabilities consistently favour a late 17th or early 16th century date. Ultimately, while offsets in the calibration curve most certainly exist, they are unlikely to dramatically affect the longstanding debate on the timing of this event.

Supplementary material. To view supplementary material for this article, please visit https://doi.org/10.1017/RDC.2025.10186.

Data availability. Some of the data used in this study are derived from public domain resources. Additional data are available within the article and its supplementary materials.

Acknowledgments. The first author was supported by the Dutch Research Council (NWO, Grant No. PGW.21.013). All of the radiocarbon analyses as well as the project members at the University of Groningen were funded by the European Research Council project, ECHOES (ERC, Grant No. 714679). The authors would like to thank the laboratory staff at the Centre for Isotope Research, Groningen for their support.

Funding Statement. Open access funding provided by University of Groningen.

References

Aydar E, Çiner A, Ersoy O, ÉCochard E and Fouache EG (2021) Volcanic ash and tsunami record of the Minoan Late Bronze Age eruption (Santorini) in a distal setting, southwestern Turkey. *Journal of Quaternary Science* **36**(4), 586–597.

Bard E, Miramont C, Capano M, Guibal F, Marschal C, Rostek F, Tuna T, Fagault Y and Heaton TJ (2023) A radiocarbon spike at 14,300 cal yr BP in subfossil trees provides the impulse response function of the global carbon cycle during the Late Glacial. *Philosophical Transactions of the Royal Society A* **381**(2261), 20220206.

Beasley RS and Klemmedson JO (1980) Ecological relationships of bristlecone pine. *American Midland Naturalist* **104**(2), 242–252.

Bietak M (2013) Antagonisms in historical and radiocarbon chronology. In Shortland AJ and Bronk Ramsey C (eds), *Radiocarbon and the Chronologies of Ancient Egypt*. Oxbow Books, 76–109.

Brehm N, Bayliss A, Christl M, Synal HA, Adolphi F, Beer J, Kromer B, Muscheler R, Solanki SK, Usoskin I and Bleicher N (2021) Eleven-year solar cycles over the last millennium revealed by radiocarbon in tree rings. *Nature Geoscience* **14**(1), 10–15.

Brehm N, Christl M, Knowles TD, Casanova E, Evershed RP, Adolphi F, Muscheler R, Synal HA, Mekhaldi F, Paleari CI and Leuschner HH (2022) Tree-rings reveal two strong solar proton events in 7176 and 5259 BCE. *Nature Communications* **13**(1), 1196.

Brehm N, Pearson CL, Christl M, Bayliss A, Nicolussi K, Pichler T, Brown D and Wacker L (2025) Tracing ancient solar cycles with tree rings and radiocarbon in the first millennium BCE. *Nature Communications* **16**(1), 406.

Bronk Ramsey C (2009a) Bayesian analysis of radiocarbon dates. *Radiocarbon* **51**(1), 337–326.

Bronk Ramsey C (2009b) Dealing with outliers and offsets in radiocarbon dating. *Radiocarbon* **51**(3), 1023–1045.

Bruins HJ, MacGillivray JA, Synolakis CE, Benjamini C, Keller J, Kisch HJ, Klügel A and van der Plicht J (2008) Geoarchaeological tsunami deposits at Palaikastro (Crete) and the Late Minoan IA eruption of Santorini. *Journal of Archaeological Science* **35**(1), 191–212.

Bruins HJ and van der Plicht J (2014) The Thera olive branch, Akrotiri (Thera) and Palaikastro (Crete): Comparing radiocarbon results of the Santorini eruption. *Antiquity* **88**(339), 282–287.

Büntgen U, Wacker L, Galván JD, Arnold S, Arseneault D, Baillie M, Beer J, Bernabei M, Bleicher N, Boswijk G and Bräuning A (2018) Tree rings reveal globally coherent signature of cosmogenic radiocarbon events in 774 and 993 CE. *Nature Communications* **9**(1), 3605.

Capano M, Miramont C, Guibal F, Kromer B, Tuna T, Fagault Y and Bard E (2018) Wood ^{14}C dating with AixMICADAS: Methods and application to tree-ring sequences from the Younger Dryas event in the southern French Alps. *Radiocarbon* **60**(1), 51–74.

Dee MW, Brock F, Harris SA, Ramsey CB, Shortland AJ, Higham TF and Rowland JM (2010) Investigating the likelihood of a reservoir offset in the radiocarbon record for ancient Egypt. *Journal of Archaeological Science* **37**(4), 687–693.

Dee MW, Palstra SWL, Aerts-Bijma AT, Bleeker MO, De Bruijn S, Ghebru F, Jansen HG, Kuitems M, Paul D, Richie RR and Spriensma JJ (2020) Radiocarbon dating at Groningen: new and updated chemical pretreatment procedures. *Radiocarbon* **62**(1), 63–74.

Driessen J (2019) The Santorini eruption. An archaeological investigation of its distal impacts on Minoan Crete. *Quaternary International* **499**, 195–204.

Driessen J and MacDonald CF (2000) The eruption of the Santorini volcano and its effects on Minoan Crete. *Geological Society, London, Special Publications* **171**(1), 81–93.

Druitt TH, McCoy FW and Vougioukalakis GE (2019) The Late Bronze Age eruption of Santorini volcano and its impact on the ancient Mediterranean world. *Elements: An International Magazine of Mineralogy, Geochemistry, and Petrology* **15**(3), 185–190.

Foster KP, Ritner RK and Foster BR (1996) Texts, storms, and the Thera eruption. *Journal of Near Eastern Studies* **55**(1), 1–14.

Friedrich R, Kromer B, Wacker L, Olsen J, Remmele S, Lindauer S, Land A and Pearson C (2020) A new annual ^{14}C dataset for calibrating the Thera eruption. *Radiocarbon* **62**(4), 953–961.

Friedrich WL, Kromer B, Friedrich M, Heinemeier J, Pfeiffer T and Talamo S (2006) Santorini eruption radiocarbon dated to 1627–1600 BC. *Science* **312**(5773), 548–548.

Friedrich WL and Sigalas N (2009) The effects of the Minoan eruption. In Warburton DA (ed), *Time's Up! Dating the Minoan Eruption of Santorini: Acts of the Minoan Eruption Chronology Workshop, Sandbjerg, November 2007* **10**, 91–100. Aarhus Universitetsforlag.

Höflmayer F (2012) The date of the Minoan Santorini eruption: Quantifying the "offset". *Radiocarbon* **54**(3–4), 435–448.

Hogg AG, Heaton TJ, Hua Q, Palmer JG, Turney CS, Southon J, Bayliss A, Blackwell PG, Boswijk G, Ramsey CB and Pearson C (2020) SHCal20 Southern Hemisphere calibration, 0–55,000 years cal BP. *Radiocarbon* **62**(4), 759–778.

Hoper ST, McCormac FG, Hogg AG, Higham TF and Head M (1997) Evaluation of wood pretreatments on oak and cedar. *Radiocarbon* **40**(1), 45–50.

Hua Q, Barbetti M and Rakowski AZ (2013) Atmospheric radiocarbon for the period 1950–2010. *Radiocarbon* **55**(4), 2059–2072.

Hua Q, Turnbull JC, Santos GM, Rakowski AZ, Ancapichún S, De Pol-Holz R, Hammer S, Lehman SJ, Levin I, Miller JB and Palmer JG (2022) Atmospheric radiocarbon for the period 1950–2019. *Radiocarbon* **64**(4), 723–745.

Jędrzejowski M, Michczyńska DJ, Kłusek M, Michczyński A, Pawełczyk F, Piotrowska N, Heeb KW and Hajdas I (2024) Radiocarbon dating of highly degraded and problematic fossil wood: Verification of the effectiveness of various preparation methods. *Radiocarbon* **66**, 1–18.

Johnston EN, Sparks RSJ, Phillips JC and Carey S (2014) Revised estimates for the volume of the Late Bronze Age Minoan eruption, Santorini, Greece. *Journal of the Geological Society* **171**(4), 583–590.

Khumalo WH, Svarva HL, Zurbach D and Nadeau MJ (2024) Squeaky clean cellulose: Comparing pretreatment effectiveness on single tree rings and wooden laths. *Radiocarbon* **66**(5), 1200–1212.

Kitagawa H, Mukai H, Nojiri Y, Shibata Y, Kobayashi T, Nojiri T (2004) Seasonal and secular variations of atmospheric 14CO2 over the Western Pacific since 1994. *Radiocarbon* **46**(2), 901–910.

Kromer B, Manning SW, Kuniholm PI, Newton MW, Spurk M and Levin I (2001) Regional $^{14}CO_2$ offsets in the troposphere: magnitude, mechanisms, and consequences. *Science* **294**(5551), 2529–2532.

Kromer B, Wacker L, Friedrich M, Lindauer S, Friedrich R, Bitterli J, Treydte K, Fonti P, Martínez-Sancho E and Nievergelt D (2024) Origin and age of carbon in the cellulose of mid-latitude tree rings. *Radiocarbon* **66**(6), 1898–1913.

Kuitems M, Panin A, Scifo A, Arzhantseva I, Kononov Y, Doeve P, Neocleous A and Dee M (2020a) Radiocarbon-based approach capable of subannual precision resolves the origins of the site of Por-Bajin. *Proceedings of the National Academy of Sciences* **117**(25), 14038–14041.

Kuitems M, van der Plicht J and Jansma E (2020b) Wood from the Netherlands around the time of the Santorini eruption dated by dendrochronology and radiocarbon. *Radiocarbon* **62**(4), 963–967.

Kuitems M, Wallace BL, Lindsay C, Scifo A, Doeve P, Jenkins K, Lindauer S, Erdil P, Ledger PM, Forbes V and Vermeeren C (2022) Evidence for European presence in the Americas in AD 1021. *Nature* **601**(7893), 388–391.

Kutschera W (2020) On the enigma of dating the Minoan eruption of Santorini. *Proceedings of the National Academy of Sciences* **117**(16), 8677–8679.

LaMoreaux PE (1995) Worldwide environmental impacts from the eruption of Thera. *Environmental Geology* **26**, 172–181.

Lange TE, Nordby JA, Murphy PL, Hodgins GW and Pearson CL (2019) A detailed investigation of pretreatment protocols for high precision radiocarbon measurements of annual tree-rings. *Nuclear Instruments and Methods in Physics Research Section B: Beam Interactions with Materials and Atoms* **15**(455), 230–233.

Lespez L, Lescure S, Saulnier-Copard S, Glais A, Berger JF, Lavigne F, Pearson C, Virmoux C, Müller Celka S and Pomadère M (2021) Discovery of a tsunami deposit from the Bronze Age Santorini eruption at Malia (Crete): Impact, chronology, extension. *Scientific Reports* **11**(1), 15487.

Levin I and Kromer B (2004) The tropospheric $^{14}CO_2$ level in mid-latitudes of the Northern Hemisphere (1959–2003) *Radiocarbon* **46**(3), 1261–1272

Luce JV and Bolton K (1976) Thera and the devastation of Minoan Crete: A new interpretation of the evidence. *American Journal of Archaeology* **80**(1), 9–18.

Maczkowski A, Pearson C, Francuz J, Giagkoulis T, Szidat S, Wacker L, Bolliger M, Kotsakis K and Hafner A (2024) Absolute dating of the European Neolithic using the 5259 BC rapid ^{14}C excursion. *Nature Communications* **15**(1), 4263.

Manning SW (2014) *A Test of Time and A Test of Time Revisited: The Volcano of Thera and the Chronology and History of the Aegean and East Mediterranean in the Mid-Second Millennium BC*. Oxford and Philadelphia: Oxbow Books.

Manning SW (2022) Second Intermediate Period date for the Thera (Santorini) eruption and historical implications. *PLOS ONE* **17**(9), e0274835.

Manning SW (2024a) Problems of dating spread on radiocarbon calibration curve plateaus: The 1620–1540 BC example and the dating of the Therasia olive shrub samples and Thera volcanic eruption. *Radiocarbon* **66**(2), 341–370.

Manning SW (2024b) Thera, the Aegean, Egypt, the Hyksos and Anatolia: Rethinking the orthodox synchronisations and histories. *Journal of Greek Archaeology* **9**, 235–276.

Manning SW, Griggs C, Lorentzen B, Bronk Ramsey C, Chivall D, Jull AT and Lange TE (2018) Fluctuating radiocarbon offsets observed in the southern Levant and implications for archaeological chronology debates. *Proceedings of the National Academy of Sciences* **115**(24), 6141–6146.

Manning SW, Höflmayer F, Moeller N, Dee MW, Ramsey CB, Fleitmann D, Higham T, Kutschera W, and Wild EM (2014) Dating the Thera (Santorini) eruption: Archaeological and scientific evidence supporting a high chronology. *Antiquity* **88**(342), 1164–1179.

Manning SW, Kromer B, Cremaschi M, Dee MW, Friedrich R, Griggs C and Hadden CS (2020a) Mediterranean radiocarbon offsets and calendar dates for prehistory. *Science Advances* **6**(12), eaaz1096.

Manning SW, Ramsey CB, Kutschera W, Higham T, Kromer B, Steier P and Wild EM (2006) Chronology for the Aegean Late Bronze Age 1700–1400 BC. *Science* **312**(5773), 565–569.

Manning, SW, and Sewell DA (2002) Volcanoes and history: A significant relationship? The case of Santorini. In Torrance R and Grattan JP (eds), *Natural Disasters and Cultural Change*. London: Routledge, 264–291.

Manning SW, Wacker L, Büntgen U, Bronk Ramsey C, Dee MW, Kromer B, Lorentzen B and Tegel W (2020b) Radiocarbon offsets and old world chronology as relevant to Mesopotamia, Egypt, Anatolia and Thera (Santorini). *Scientific Reports* **10**(1), 13785.

Marinatos S (1939) The volcanic destruction of Minoan Crete. *Antiquity* **13**(52), 425–439.

McCoy FW and Heiken G (2000) Tsunami generated by the Late Bronze Age eruption of Thera (Santorini), Greece. *Pure and Applied Geophysics* **157**, 1227–1256.

McCoy FW (2009) The eruption within the debate about the date. In Warburton DA (ed), *Time's Up! Dating the Minoan Eruption of Santorini: Acts of the Minoan Eruption Chronology Workshop, Sandbjerg, November 2007* **10**, 91. Aarhus Universitetsforlag.

McDonald L, Chivall D, Miles D and Ramsey CB (2019) Seasonal variations in the ^{14}C content of tree rings: Influences on radiocarbon calibration and single-year curve construction. *Radiocarbon* **61**(1), 185–194.

Miyake F, Masuda K, Nakamura T (2013) Another rapid event in the carbon-14 content of tree rings. *Nature Communications* **4**(1), 1748.

Miyake F, Nagaya K, Masuda K and Nakamura T (2012) A signature of cosmic-ray increase in AD 774–775 from tree rings in Japan. *Nature* **486**(7402), 240–242.

Miyake F, Panyushkina IP, Jull AJT, Adolphi F, Brehm N, Helama S, Kanzawa K, Moriya T, Muscheler R, Nicolussi K and Oinonen M (2021) A single-year cosmic ray event at 5410 BCE registered in ^{14}C of tree rings. *Geophysical Research Letters* **48**(11), e2021GL093419.

O'Hare P, Mekhaldi F, Adolphi F, Raisbeck G, Aldahan A, Anderberg E, Beer J, Christl M, Fahrni S, Synal HA and Park J (2019) Multiradionuclide evidence for an extreme solar proton event around 2,610 BP (~660 BC) *Proceedings of the National Academy of Sciences* **116**(13), 5961–5966.

Panyushkina IP, Jull AT, Molnár M, Varga T, Kontul' I, Hantemirov R, Kukarskih V, Sljusarenko I, Myglan V and Livina V (2024) The timing of the ca-660 BCE Miyake solar-proton event constrained to between 664 and 663 BCE. *Communications Earth & Environment* **5**(1), 454.

Park J, Southon J, Fahrni S, Creasman PP and Mewaldt R (2017) Relationship between solar activity and Δ^{14}C peaks in AD 775, AD 994, and 660 BC. *Radiocarbon* **59**(4), 1147–1156.

Pearson C, Salzer M, Wacker L, Brewer P, Sookdeo A and Kuniholm P (2020a) Securing timelines in the ancient Mediterranean using multiproxy annual tree-ring data. *Proceedings of the National Academy of Sciences* **117**(15), 8410–8415.

Pearson C, Sbonias K, Tzachili I and Heaton TJ (2023) Olive shrub buried on Therasia supports a mid-16th century BCE date for the Thera eruption. *Scientific Reports* **13**(1), 6994.

Pearson C, Wacker L, Bayliss A, Brown D, Salzer M, Brewer P, Bollhalder S, Boswijk G and Hodgins G (2020b) Annual variation in atmospheric ^{14}C between 1700 BC and 1480 BC. *Radiocarbon* **62**(4), 939–952.

Pearson CL, Brewer PW, Brown D, Heaton TJ, Hodgins GW, Jull AJT, Lange T and Salzer MW (2018) Annual radiocarbon record indicates 16th century BCE date for the Thera eruption. *Science Advances* **4**(8), eaar8241.

Pyle DM (1997) The global impact of the Minoan eruption of Santorini, Greece. *Environmental Geology* **30**, 59–61.

Regev J, Gadot Y, Uziel J, Chalaf O, Shalev Y, Roth H, Shalom N, Szanton N, Bocher E, Pearson CL and Brown DM (2024) Radiocarbon chronology of Iron Age Jerusalem reveals calibration offsets and architectural developments. *Proceedings of the National Academy of Sciences* **121**(19), e2321024121.

Reimer PJ, Austin WE, Bard E, Bayliss A, Blackwell PG, Ramsey CB, Butzin M, Cheng H, Edwards RL, Friedrich M and Grootes PM (2020) The IntCal20 Northern Hemisphere radiocarbon age calibration curve (0–55 cal kBP) *Radiocarbon* **62**(4), 725–757.

Rinne KT, Boettger T, Loader NJ, Robertson I, Switsur VR and Waterhouse JS (2005) On the purification of α-cellulose from resinous wood for stable isotope (H, C, and O) analysis. *Chemical Geology* **222**(1–2), 75–82.

Şahoğlu V, Sterba JH, Katz T, Çayır Ü, Gündoğan Ü, Tyuleneva N, Tuğcu İ, Bichler M, Erkanal H and Goodman-Tchernov BN (2022) Volcanic ash, victims, and tsunami debris from the Late Bronze Age Thera eruption discovered at Çeşme-Bağlararası (Turkey) *Proceedings of the National Academy of Sciences* **119**(1), e2114213118.

Scifo A, Abi Nassif T, Conti M, Bayliss A, Doeve P and Dee MW (2024) New data fails to replicate the small-scale radiocarbon anomalies in the early second millennium CE. *Radiocarbon* **66**(3), 518–531.

Sharma U, Zhang Q and Dennis J (2023) ticktack: A Python package for carbon box modelling. *Journal of Open Source Software* **8**(83), 5084.

Sigurdsson H, Carey S, Alexandri M, Vougioukalakis G, Croff K, Roman C, Sakellariou D, Anagnostou C, Rousakis G, Ioakim C and Goguo A (2006) Marine investigations of Greece's Santorini volcanic field. *Eos, Transactions American Geophysical Union* **87**(34), 337–342.

Soles JS (2007) The impact of the Minoan eruption of Santorini on Mochlos, a small Minoan town on the north coast of Crete. *Monographs of the Danish Institute at Athens (MoDIA)* **10**, 107–116.

Synal HA, Stocker M and Suter M (2007) MICADAS: A new compact radiocarbon AMS system. *Nuclear Instruments and Methods in Physics Research Section B: Beam Interactions with Materials and Atoms* **259**(1), 7–13.

Ward GK and Wilson SR (1978) Procedures for comparing and combining radiocarbon age determinations: A critique. *Archaeometry* **20**, 19–31.

Warren P and Hankey V (1989) *Aegean Bronze Age Chronology*. Bristol Classical Press.

Warren P (2010) The absolute chronology of the Aegean circa 2000 BC–1400 BC: A summary. In Müller W (ed), Die Bedeutung der minoischen und mykenischen Glyptik: VI. Internationales Siegel-Symposium aus Anlass des 50 jährigen Bestehens des CMS, Marburg, 9.-12. Oktober 2008 (CMS Beiheft 8) Verlag Philipp von Zabern, Mainz am Rhein, Vol. 50, 383–394.

Warren P (2009) The date of the Late Bronze Age eruption of Santorini. In Warburton DA (ed), *Time's Up! Dating the Minoan Eruption of Santorini: Acts of the Minoan Eruption Chronology Workshop, Sandbjerg, November 2007* **10**, 181–186. Aarhus Universitetsforlag.

White RS and Humphreys CJ (1994) Famines and cataclysmic volcanism. *Geology Today* **10**(5), 181–185.

Zhang Q, Sharma U, Dennis JA, Scifo A, Kuitems M, Büntgen U, Owens MJ, Dee MW and Pope BJ (2022) Modelling cosmic radiation events in the tree-ring radiocarbon record. *Proceedings of the Royal Society A* **478**(2266), 20220497.

Cite this article: Erdil P, Kuitems M, Scifo A, Brown D, and Dee MW (2026). Investigating potential radiocarbon anomalies around the time of the Minoan eruption of Thera: A new high-resolution dataset from Groningen. *Radiocarbon* **68**, 264–280. https://doi.org/10.1017/RDC.2025.10186